

Discovery of Potent and Orally Bioavailable Small Molecule Antagonists of Toll-like Receptors 7/8/9 (TLR7/8/9)

Christopher P. Mussari, Dharmapal S. Dodd, Ratna Kumar Sreekantha, Laxman Pasunoori, Honghe Wan, Shana L. Posy, David Critton, Stefan Ruepp, Murali Subramanian, Andrew Watson, Paul Davies, Gary L. Schieven, Luisa M. Salter-Cid, Ratika Srivastava, Debarati Mazumder Tagore, Shailesh Dudhgaonkar, Michael A. Poss, Percy H. Carter, and Alaric J. Dyckman*

Cite This: *ACS Med. Chem. Lett.* 2020, 11, 1751–1758

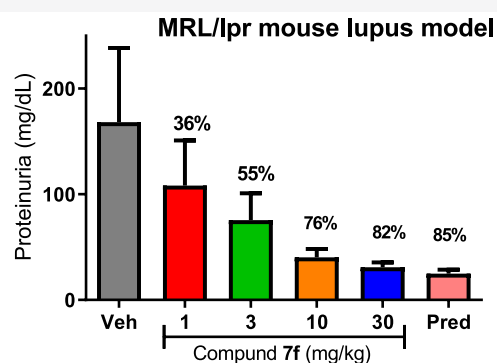
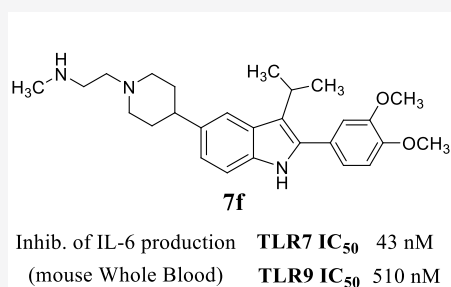
Read Online

ACCESS |

Metrics & More

Article Recommendations

Supporting Information



ABSTRACT: The toll-like receptor (TLR) family is an evolutionarily conserved component of the innate immune system, responsible for the early detection of foreign or endogenous threat signals. In the context of autoimmunity, the unintended recognition of self-motifs as foreign promotes initiation or propagation of disease. Overactivation of TLR7 and TLR9 have been implicated as factors contributing to autoimmune disorders such as psoriasis, arthritis, and lupus. In our search for small molecule antagonists of TLR7/9, **7f** was identified as possessing excellent on-target potency for human TLR7/9 as well as for TLR8, with selectivity against other representative TLR family members. Good pharmacokinetic properties and a relatively balanced potency against TLR7 and TLR9 in mouse systems (systems which lack functional TLR8) made this an excellent *in vivo* tool compound, and efficacy from oral dosing in preclinical models of autoimmune disease was demonstrated.

KEYWORDS: Toll-like receptor, TLR, autoimmunity, innate immunity, psoriasis, lupus

The innate immune system, a first line of host-defense, includes several families of pattern recognition receptors (PRRs) such as the Toll-like receptor (TLR) family. PRRs recognize pathogen-associated molecular patterns (PAMPs) from invading microbes and danger-associated molecular patterns (DAMPs) released from stressed or damaged host cells.¹ TLRs are transmembrane proteins composed of an extracellular (or intraendosomal) ligand-binding domain connected via a transmembrane region to a cytosolic toll/interleukin (TIR) signaling domain.² Binding of ligands (PAMPs/DAMPs) to the ectodomain (ECD) of hetero- or homodimeric TLR pairs initiates signaling events via recruitment of adaptor proteins to the TIR domain. This activates signal transduction cascades resulting in cellular proliferation as well as production of type-I interferons (IFN) and other pro-inflammatory cytokines and chemokines. To date, 13 mammalian TLRs have been identified, including nine subtypes (TLR1–9) with defined functions in human.²

These PRRs are localized either on the plasma cell membrane (TLR1, 2, 4, 5, 6) or on endosomal membranes (TLR3, 7, 8, 9), with the endosomal TLRs responding to double-stranded RNA (TLR3), single-stranded RNA (TLR7 and 8), or hypomethylated double-stranded DNA (TLR9) as activating ligands. In autoimmune disorders, sustained activation of TLR7/9 has been shown to play a key role in immune dysfunction, leading to enhanced disease states.³ In mouse models, overexpression of TLR7 led to autoimmune disease progression, while TLR7 deficiency protected against disease

Received: June 12, 2020

Accepted: July 29, 2020

Published: July 29, 2020



development in the lupus-prone MRL/lpr background.^{4,5} Although specific knockout of TLR9 led to worsening of disease in lupus-prone mice, the dual knockout of TLR7 and 9 again showed enhanced protection, supporting the potential benefit of dual inhibition of these targets for the treatment of lupus.⁶ Among the other endosomal TLRs, TLR3 signaling has not been as strongly associated with autoimmune disorders, while deciphering the role of TLR8 has been complicated by species differences. Unlike TLR7 or TLR9, the roles of TLR8 in humans are not recapitulated in mouse—mouse TLR8 does not respond to single-stranded RNA ligands, which do stimulate TLR8 in human.^{4,7} As such, an understanding of the function of TLR8 in autoimmune diseases has lagged behind that of other TLRs.⁸

Herein, we detail the identification of potent and selective small molecule antagonists of TLR7/8/9 based on a 2-phenyl-indole chemical series. While TLR8 function is not captured in mouse models, the *in vivo* studies presented here support at least the potential utility of small molecule antagonists of TLR7/9 as therapeutics for the treatment of autoimmune disorders. Examples of potent small molecule inhibitors of endosomal TLR signaling were quite limited at the outset of our efforts, with none showing the desired TLR selectivity profile that we were seeking.⁹ Antimalarials (e.g., chloroquine, quinacrine) and structurally related compounds have been shown to inhibit TLR9 but were reported to exert their effects through binding to the nucleic acid ligands, resulting in limited selectivity against TLR3 as well as inhibition of other cytosolic DNA sensors.^{10,11} We initiated a screen of a proprietary compound collection utilizing cellular reporter assays to monitor for inhibition of TLR activity, focused on the identification of antagonists of TLR7 and TLR9, given the body of data connecting their dysregulation to autoimmune disorders. The screen utilized the HEK293 Blue secreted embryonic alkaline phosphatase (SEAP) assay,¹² in which the cells were engineered to overexpress the TLRs of interest. The functional nature of this screen necessitated deconvolution to filter out general pathway inhibitors with alternative mechanisms of action. Counter-screening against additional endosomal (TLR3) and cell-surface (TLR4) family members helped to eliminate nonspecific pathway inhibitors or compounds with assay interference.

Given the human-to-mouse TLR8 functional disconnect discussed above, activity on that receptor was not tracked for all compounds, with only advanced examples subsequently evaluated. From these screening efforts, a 2-phenyl-indole-5-piperidine chemical series was identified, with examples demonstrating encouraging dual antagonism of TLR7/9 and an indication that selectivity against TLR3/4 could be achieved (Figure 1, 4a,b). This scaffold afforded an opportunity to readily investigate changes to several positions, including at N-1, on the C-2 phenyl, at C-3, and the nitrogen of the C-5 piperidine.

Structure–activity relationship (SAR) studies began with variation of the indole C-2 group as shown in Table 1. Mono- and disubstituted phenyl patterns were explored using both electron-donating and electron-withdrawing groups. The tolerability for substitution of the C-2 phenyl was narrow for TLR7, with unsubstituted and monosubstituted systems, regardless of substituent position or electronics, showing poor TLR7 activity. Of the single substitution patterns evaluated, a methoxy group in the *meta* or *para* positions (5f, 5g) were the most encouraging. Combination of these

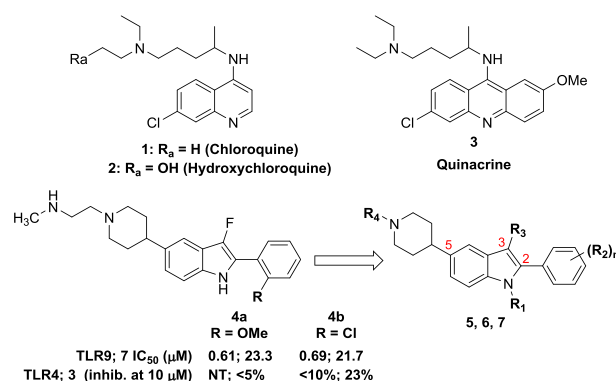


Figure 1. Indole-5-piperidine chemical series identified from screening.

Table 1. C-2 SAR of C-3-Methyl-indoles

compd	R ₁	R ₂	R ₃	TLR7 IC ₅₀ (nM) ^a	TLR9 IC ₅₀ (nM) ^a
5a	H	H	H	>10000	1800 ± 820
5b	Me	H	H	>10000	2140 ± 1150
5c	H	Me	H	>10000	2620 ± 1550
5d	H	H	Me	>10000	5390 ± 3770
5e	OMe	H	H	>10000	1100*
5f	H	OMe	H	6170 ± 1200	1870 ± 1360
5g	H	H	OMe	5460 ± 960	500 ± 420
5h	CN	H	H	>10000*	600*
5i	H	CN	H	>10000	460 ± 130
5j	H	H	CN	7010 ± 220	520 ± 210
5k	H	H	CONH ₂	16600*	270 ± 60
5l	OMe	H	OMe	>10000	2330 ± 420
5m	OMe	OMe	H	>10000	2200 ± 690
5n	H	OMe	OMe	250 ± 160	430 ± 260
5o	H	OEt	OiPr	5550*	1660*
5p				650 ± 100	1205 ± 470

^aIC₅₀ values are a mean of two or more individual determinations except those marked with *.

substitutions into the 3',4'-dimethoxyphenyl compound 5n provided a dramatic improvement in TLR7 potency. Constraining these substituents as in dioxolane 5p reduced TLR7 activity, as did increasing the size of the alkoxy groups, as in 5o. Specific positioning of the dimethoxy groups was critical, with the 2',4'- (5l) and 2',3'-dimethoxy (5m) patterns yielding substantially reduced TLR7 activity.

Activity against TLR9 was more accommodating to changes in C-2 phenyl substitution, although the SAR was flat in comparison to TLR7 activity. Across the range of changes described in Table 1, at least modest TLR9 antagonism was retained, spanning a range of approximately 300–5000 nM. Single substitutions at any position of the C-2 phenyl with a methyl group led to a slight (3-fold or less) decrease in activity, whereas introduction of a methoxy group was most advanta-

geous when placed at the *para* position (**5g**). Nitrile substitution was also beneficial for TLR9 activity, regardless of position (**5h–j**). An additional electron withdrawing group, the primary carboxamide, was explored only at the *para* position, providing further improved activity (**5k**). For the disubstituted examples, the 3',4'-dimethoxy provided favorable results, as was observed for TLR7 activity (**5n**). The constrained (**5p**) and bulkier (**5o**) analogues were once again found to exhibit reduced activity relative to the 3',4'-dimethoxy substitution pattern.

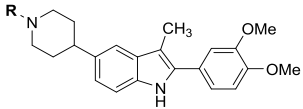
Compound **5n** was profiled for selectivity and exhibited reduced activity against TLR3 (IC₅₀ 2160 nM) and TLR4 (IC₅₀ 14970 nM) relative to TLR7/9. On the basis of the encouraging dual 7/9 antagonist profile of **5n**, the 3',4'-dimethoxyphenyl group was retained at C-2 for subsequent studies. Efforts turned to the evaluation of C-5 piperidine capping groups (Table 2). In comparison to the relatively steep

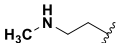

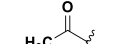
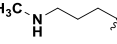
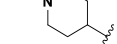
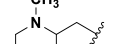
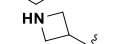
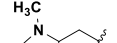
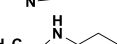
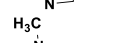
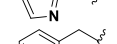
Acetylation of the piperidine to afford a nonbasic C-5 group (**6b**) was somewhat detrimental to TLR7 activity (5-fold reduced vs **5n**) but highly detrimental to TLR9 activity (IC₅₀ > 50 000 nM). The spacing between the basic atoms and nature of their arrangement was flexible, as highlighted by examples **6c–6f**. Homologated compound **6c** demonstrated activity against both TLRs that was close to that of **5n**, particularly for TLR9. Cyclic constraint of the terminal amine chain such as piperidines **6d** and **6e** were comparable in activity to homologated **6c**. As compared to the piperidine (**6d**), constraint as an azetidines (**6f**) led to slightly reduced TLR7 activity (~2-fold) but TLR9 potency was 10-fold reduced, possibly corresponding to the reduction in pK_a of both amines introduced by this moiety.

The remaining compounds in Table 2 describe the effects of introducing a pendant heteroaryl group off of the piperidine nitrogen via a methylene linker. In each case, the basicity of the piperidine nitrogen is attenuated by the substituent, which includes a second nitrogen of varying basicity. While 1-methyl-5-yl-imidazole **6g** showed modest activity for TLR7 and TLR9, 2-methylimidazole **6h** was 4-fold reduced in TLR7 potency but demonstrated very good TLR9 activity despite only a slight change in calculated basicity of these constitutional isomers. Imidazole **6i**, regioisomeric to **6g**, also exhibited reduced TLR7 but increased TLR9 activity despite a reduction in calculated pK_a values.

Compound **5n** also served as the basis for optimization at the N-1 and C-3 indole positions (Table 3). The N-1 position

Table 2. C-5 Piperidine SAR

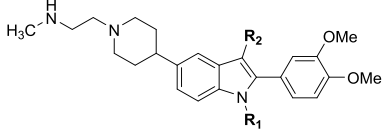


compd	pK _a ^a	R	TLR7 IC ₅₀ (nM) ^b	TLR9 IC ₅₀ (nM) ^b
5n	pK _{a1} = 10.0 pK _{a2} = 6.6		250 ± 160	430 ± 260
6a	pK _{a1} = 10.0		380 ± 250	4845 ± 3220
6b	NA		1310 ± 290	>50000
6c	pK _{a1} = 10.6 pK _{a2} = 8.0		790 ± 230	550 ± 230
6d	pK _{a1} = 10.2 pK _{a2} = 7.1		730 ± 300	216 ^c
6e	pK _{a1} = 10.0 pK _{a2} = 6.0		850 ± 480	740 ± 370
6f	pK _{a1} = 9.5 pK _{a2} = 3.0		1720 ± 1250	2340 ± 2520
6g	pK _{a1} = 8.1 pK _{a2} = 5.5		920 ± 380	2710 ± 1440
6h	pK _{a1} = 8.0 pK _{a2} = 6.2		3490 ± 1090	190 ^c
6i	pK _{a1} = 7.4 pK _{a2} = 3.8		3690 ± 2690	850 ± 920
6j	pK _{a1} = 8.6 pK _{a2} = 3.5		1680 ± 530	3360 ± 1450

^aACDpK_a calculated by Instant JChem software (ChemAxon); showing values within a range of 0–15. ^bIC₅₀ values are a mean of two or more individual determinations except those marked with *.

and unaccommodating TLR7 SAR noted for the substitution pattern of the C-2 phenyl, a high level of chemical diversity was tolerated off of the C-5 piperidine. For TLR9, the antagonist activity was noted to be influenced by the basicity of the region, specifically the number of basic atoms and the varying level of basicity associated with each. Removal of the piperidine capping group to give monobasic **6a** was tolerated for TLR7 but not for TLR9 (>10-fold reduction in activity).

Table 3. SAR of Indole N-1 and C-3 Positions



compd	R ₁	R ₂	TLR7 IC ₅₀ (nM) ^a	TLR9 IC ₅₀ (nM) ^a
5n	H	Me	250 ± 160	430 ± 260
7a	Me	Me	5260 ± 1540	740 ± 170
7b	H	Cl	1880 ± 710	430 ± 170
7c	H	CN	>10 000	260 ± 200
7d	H	CH ₂ CH ₃	130 ± 100	490 ± 370
7e	H	CH ₂ CF ₃	70 ± 40	750 ± 270
7f	H	isopropyl	10 ± 7	700 ± 390
7g	H	isobutyl	1290 ± 770	830 ± 770

^aIC₅₀ values are a mean of two or more individual determinations.

was found to be intolerant to substitution in regards to TLR7 activity as evidenced by methyl indole **7a** (IC₅₀ 5260 nM), whereas TLR9 activity was only slightly reduced by this change (IC₅₀ 740 nM). Modification of the C-3 position proved much more rewarding, with a range of variations being well tolerated for TLR9 activity and select changes leading to dramatic improvement in TLR7 potency. While chloro (**7b**) or cyano (**7c**) replacements at C-3 reduced TLR7 activity, extension of the alkyl group to ethyl (**7d**) or trifluoroethyl (**7e**) improved TLR7 activity by 2- to 4-fold. This improvement was even more pronounced with isopropyl substituted **7f**, which provided low nanomolar TLR7 potency (IC₅₀ 10 nM). Homologation to isobutyl substitution (**7g**) led to a precipitous decline in TLR7 potency (IC₅₀ 1290 nM), although that extension had little effect on TLR9 activity.

As described above, **7f** was found to be a potent antagonist of TLR7 with modest activity against TLR9. Further evaluation against other TLRs in the HEK293 reporter system (Table 4)

Table 4. TLR Cellular and Whole Blood Activity Data for 7f

assay	receptor	IC ₅₀ (nM) ^a
HEK293; NF-κB reporter (antagonist mode)	TLR9	700 ± 390
	TLR8	17 ± 37
	TLR7	10 ± 7
	TLR4	15100 ± 16500
	TLR3	5440 ± 5000
HEK293; NF-κB reporter (agonist mode)	TLR7,8,9	>50000
PBMCs; IL-6	TLR9	510 ± 80
	TLR7	4.8 ± 3.6
pDC (ODN2216); IFN α pDC (flu virus); IFN α	TLR9	210 ± 390
	TLR7	11 ± 9
human whole blood; IL-6	TLR9	320 ± 97
	TLR8	5.1 ± 5.6
	TLR7	5.7 ± 6.3
mouse whole blood; IL-6	TLR9	510 ± 150
	TLR7	43 ± 45

^aIC₅₀ values are a mean of two or more individual determinations. See Supporting Information for assay details.

showed **7f** to also possess potent activity against TLR8 (IC₅₀ 17 nM) but much reduced activity against endosomal TLR3 (IC₅₀ 5440 nM) and cell-surface TLR4 (IC₅₀ 15 100 nM). In agonist mode, **7f** was inactive up to 50 000 nM against TLR7, 8, or 9. The antagonist activity of **7f** was tested in additional cellular and whole blood assays. In a peripheral blood mononuclear cell (PBMC) assay measuring IL-6 production, inhibition of TLR7- or 9-driven responses were very similar to that observed in the HEK293 reporter assays. Inhibition of the TLR9-stimulated production of IFN α in plasmacytoid dendritic cells (pDCs) was found to be more pronounced (IC₅₀ 210 nM) than for other cellular assays. As pDCs express both TLR9 and TLR7, this cell type was also used for the evaluation of TLR7 inhibition. The TLR7 agonist employed in the pDC assay was inactivated flu virus rather than a small molecule agonist as utilized in the other assays. The excellent response of **7f** in this assay (IC₅₀ 11 nM) with a more physiologically relevant TLR7 ligand highlights that the potency appears to be independent of the nature of the TLR7 agonist. This differentiates from the antimalarials, for which poor inhibitory activity was observed against non-nucleic acid-based agonists of TLR7.¹⁰ In human whole blood (hWB) assays, **7f** demonstrated inhibition of IL-6 production consistent with the cellular responses for TLR7, 8, 9. In anticipation of in vivo studies in mouse, the activity of **7f** was evaluated in mouse whole blood (mWB) assays. As described above, TLR8 is nonfunctional in mouse, and for that reason only TLR7 and TLR9 responses were examined in this mWB assay. The TLR9 inhibitory response of **7f** in mWB (IC₅₀ 510 nM) was similar to that found in hWB, however, the TLR7 inhibition in mWB (IC₅₀ 43 nM) was ~7-fold reduced relative

to hWB, indicating a more balanced TLR7/9 dual antagonist profile in mouse.

Assessment of pharmacokinetic (PK) properties for **7f** in mouse showed good oral bioavailability (62%F) and a flat exposure profile with a 24 h peak-to-trough ratio of ~4 (Table 5). On the basis of exposures in blood, the time to maximal

Table 5. Mouse Pharmacokinetic Profile of 7f^a

	dose (mg/kg)	
	3 (IV)	15 (PO)
T _{max} (h)		0.5
C _{max} (nM)		1628
Cl (mL/min/kg)	7.7	
V _{ss} (L/kg)	20	
T _{1/2} (h)	32	
F (%)		62

^aIV vehicle: 70/30 PEG400/water. PO vehicle: 80/20 PEG400/200 mM citrate buffer (pH 3.0).

concentration (T_{max}) for oral dosing was rapid (0.5 h) with maximal concentration (C_{max}) of 1628 nM (15 mg/kg). The low clearance and high volume of distribution (20 L/kg) led to a long terminal half-life of 32 h. Compound **7f** was found to partition preferentially into the blood (blood-to-plasma ratio 4.6:1 at 2 h and 6.9:1 at 7 h) and also into the central nervous system (7 h brain to plasma ratio 1.4:1).

In mouse pharmacodynamic (PD) models, oral dosing with **7f** was able to effectively block cytokine production elicited by treatment with agonists of TLR7 (gardiquimod) or TLR9 (ODN1585) (Figure 2). A dose-dependent decrease in agonist-induced IL-6 production was observed, with plasma EC₅₀ of 2.4 nM (TLR7) or 25 nM (TLR9). This was noted to be 4- to 5-fold more potent than the mWB assay results when factoring in the blood-to-plasma ratio, possibly reflecting the preferential distribution of the compound into tissues.

7f was then advanced to rodent models of autoimmune disorders. Topical application of imiquimod (a TLR7 agonist) is a well-precedented method of eliciting skin changes characteristic of human psoriasis.¹³ In this model, imiquimod cream (5%) was applied to the shaved back region of mice once a day for 6 days, and the effect of concurrent once-daily oral treatment with **7f** was compared to dexamethasone (3 mg/kg qd) or vehicle control (Figure 3).

Significant and dose-dependent suppression of multiple end points was observed, with maximal activity of **7f** exceeding the efficacy shown by dexamethasone. As shown for the scaling end point, treatment with **7f** led to a reduction of up to ~70% relative to vehicle at the top dose. Exposures from day 5 (Supporting Information) show that achieving partial coverage above mWB TLR7 IC₅₀ as observed for the 3 mg/kg dose appears sufficient to elicit ~50% inhibition in scaling, whereas sustained coverage above the mWB IC₅₀, as achieved for the 10 and 30 mg/kg doses, provided further improvement.

Compound **7f** was subsequently progressed to a disease model with a more extensive duration of dosing. MRL/lpr mice spontaneously develop disease with manifestations that are reminiscent of human lupus, including proteinuria, lymphadenopathy, splenomegaly, elevated cytokine production, and increased antibody production.¹⁴ Figure 4 shows the effect of 8 weeks of treatment with **7f** (1, 3, 10, 30 mg/kg, qd) as compared to treatment with prednisolone (10 mg/kg, qd) on the urinary marker proteinuria (Figure 4A), antidouble-

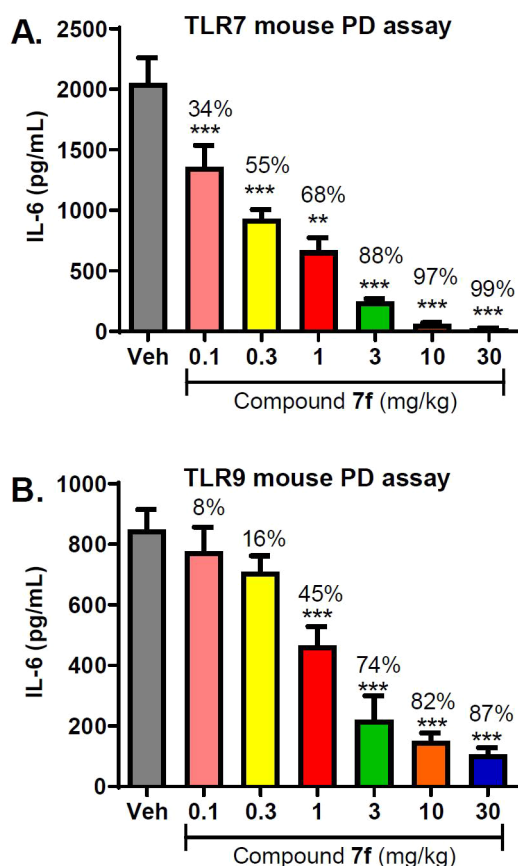


Figure 2. Efficacy of 7f in TLR7 (A) and TLR9 (B). PD experiments measuring suppression of agonist-induced IL-6. ** $p < 0.01$, *** $p < 0.001$. One-way ANOVA with Dunnett's test compared to the vehicle. $N = 8$ mice per group.

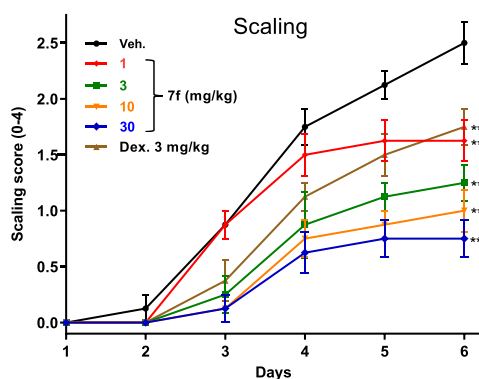


Figure 3. Efficacy of 7f (1, 3, 10, 30 mg/kg) or dexamethasone (3 mg/kg) vs vehicle in imiquimod-induced mouse model of psoriasis showing changes to scaling ** $p < 0.01$, *** $p < 0.001$. One-way ANOVA with Dunnett's test compared to the vehicle. $N = 7$ –10 mice per group.

stranded DNA (dsDNA) antibody titer (Figure 4B), and the serum cytokine IL-10 (Figure 4C) in the MRL/lpr mice.

For each end point, a dose-dependent decrease in severity was noted, with a maximal response comparable to that shown by the steroid positive control. Exposures of 7f at the end of the study (Supporting Information) indicated that sustained coverage above the mWB EC_{50} for TLR7 was achieved with a dose of 3 mg/kg, where notable impact on proteinuria (55% reduction) was observed and modest reduction (30–35%) of

the other end points was seen. At the higher doses (10, 30 mg/kg), coverage above the TLR9 mWB EC_{50} was achieved as well, and more robust efficacy was demonstrated.

Subsequent to the identification of 7f as a potent antagonist of TLR7/8/9, structural evidence was obtained informing on the direct binding mode of inhibition for this class of compounds. The availability of hTLR8 protein enabled the generation of cocrystal structures with compound 17c, as detailed in Figure 5.

TLR8 crystallized as a dimer with two symmetric ligand binding sites located at the dimer interface, consistent with previously reported TLR8 X-ray structures^{15,16} (Figure 5A,C). Interestingly, 17c stabilizes an inactive conformation of TLR8 in which the C-termini of the ECD are positioned far apart; the structure aligns well with the apo conformation of the protein (Figure 5C, middle). The open, inactive conformation observed in this study is differentiated from both the closed, active agonist-bound conformation (Figure 5C, left) and from a recently reported antagonist-bound structure, which demonstrated an inactive, moderately open conformation (Figure 5C, right).¹⁷ Figure 5B shows a detailed view of one of the binding sites. The 3',4'-dimethoxyphenyl moiety forms a bidentate hydrogen bond to the Gly-351 backbone NH and stacks between Tyr-348 of one chain and Phe-494/Phe-495 of the second chain. These interactions account for the SAR favoring the 3',4'-dimethoxy substitution pattern on the C-2 phenyl. The importance of the indole NH for activity (e.g., indole *N*-methyl 7a; TLR8 IC_{50} 958 nM) can be understood in light of the hydrogen bond between the backbone carbonyl of Phe-494 and the indole NH. The protonated piperidine is able to interact with the Glu-427 side chain and is oriented toward the solvent-exposed interior of the ectodomain, consistent with the flexible SAR observed for substitution of the C-5 position. TLR7 and TLR8 share 40% sequence identity in their ectodomains, and 50% of the residues in the 17c binding site are identical. TLR7 and TLR8 activity align well for the compounds tested, and homology modeling of the TLR7 binding site supports a similar set of protein–ligand interactions. The TLR9 ECD is related more distantly to TLR8 (33% sequence identity overall and 25% in the binding site), which is reflected in the more disparate SAR for TLR7/8 vs TLR9 inhibition.

Preparation of indole-based antagonists is depicted in Scheme 1. Variation of the C-3 position was accomplished through the use of commercially available 5-bromoindoles. The C-3 methylindole (9a) was prepared via $LiAlH_4$ reduction of 5-bromo-indole-3-carboxaldehyde (8a), while the C-3 alkyl indoles 9b–d were prepared by exposing 8b to the appropriate secondary amine in the presence of Shvo's catalyst. These indole cores 9a–d, along with the commercially available 3-cyano-5-bromoindole (9e), were further elaborated to the general structure 10 by Suzuki–Miyaura cross-coupling and subsequent hydrogenation. Preparation of C-3 chloro intermediate 10f began with cross-coupling and reduction of 5-bromoindole (8b) in a manner similar to that described above, followed by NCS-mediated chlorination. Bromination of 10a–f with NBS occurred selectively at the C-2 position to afford intermediates 11a–f, which were transformed into the final compounds by one of several routes. Functionalization of the indole C-2 position required the removal of the piperidine Boc protecting group via treatment of 11a–c with HBr/acetic acid in DCM. Addition of TEA, followed by aldehyde 12 under reductive amination conditions, afforded scaffolds 13a–c,

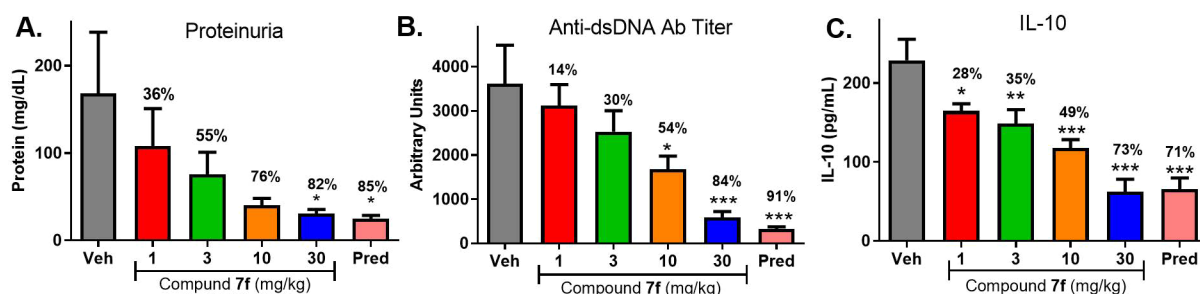


Figure 4. Efficacy of **7f** (1, 3, 10, 30 mg/kg) or prednisolone (10 mg/kg) vs vehicle in a MRL/lpr mouse model of lupus showing changes to proteinuria levels (A), anti-dsDNA antibody titer (B), and plasma IL-10 (C). * $p < 0.05$, ** $p < 0.01$, *** $p < 0.001$. One-way ANOVA with Dunnett's test compared to the vehicle. $N = 12$ mice per group.

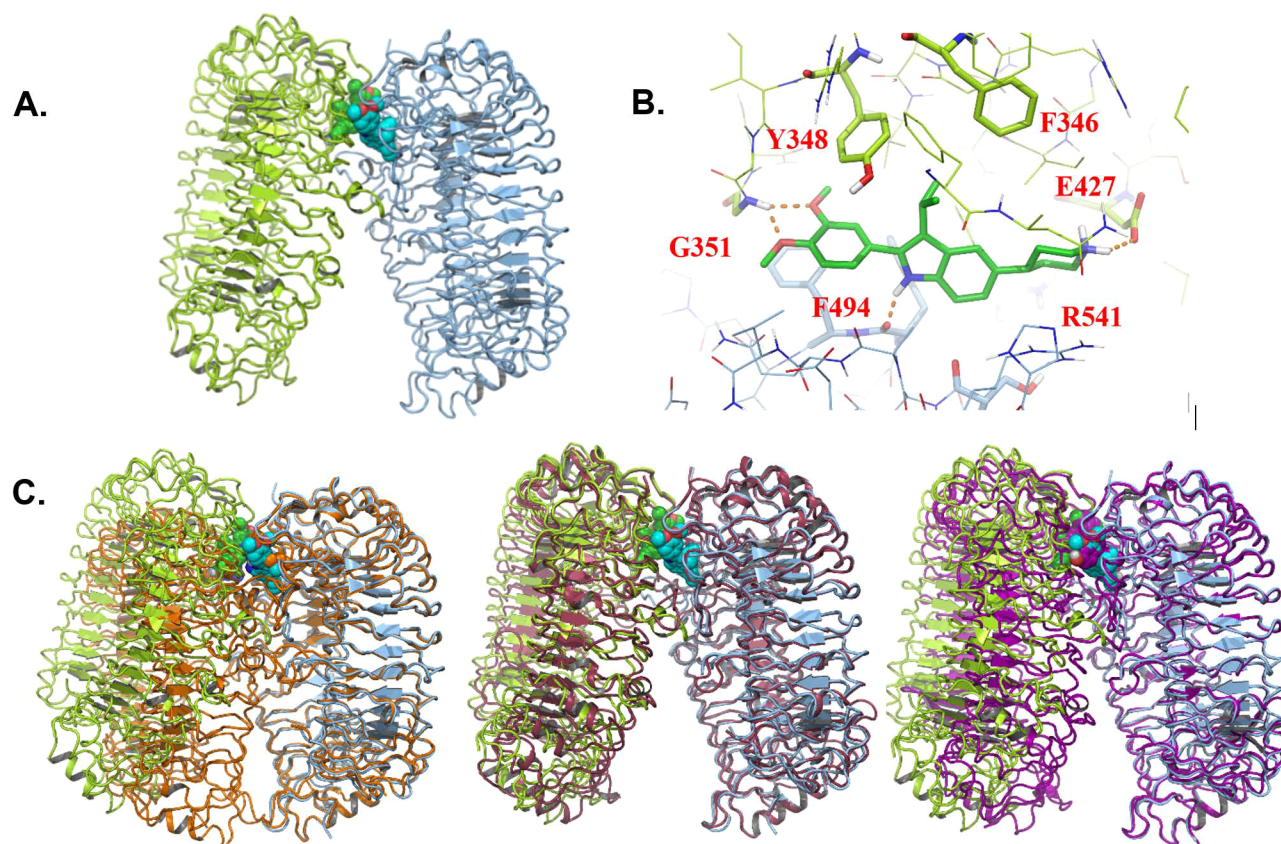


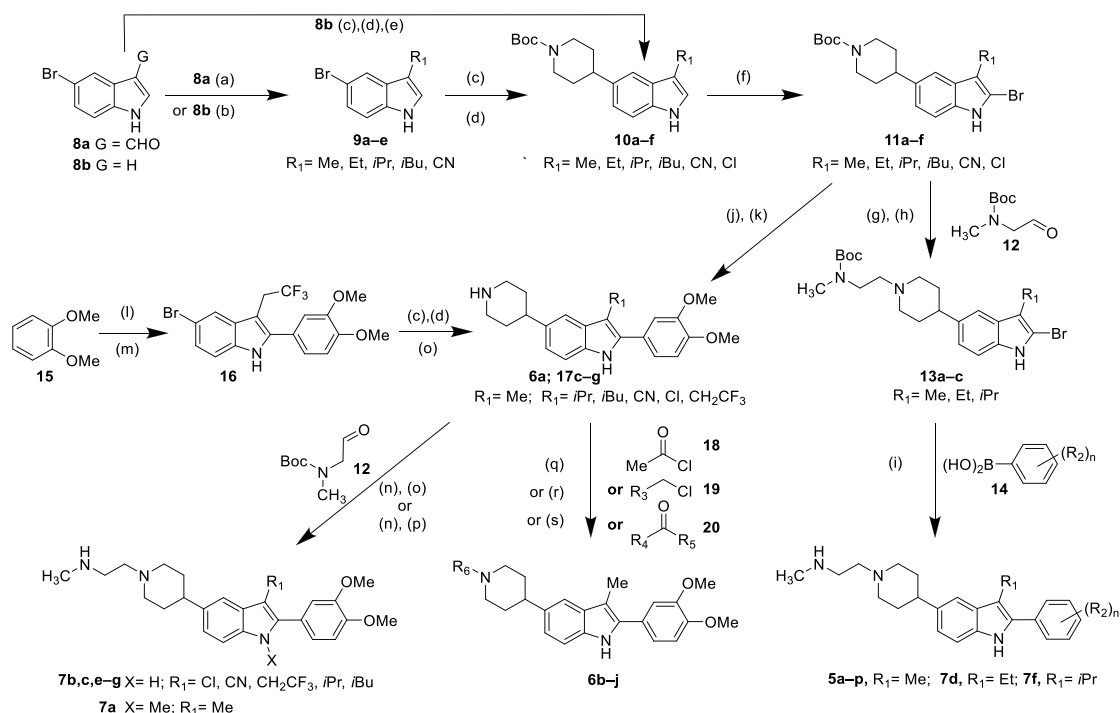
Figure 5. X-ray crystal structure of **17c** bound to TLR8. (A) Structure of **17c** in complex with human TLR8 (RCSB PDB 6V9U). The two protein chains are shown as light-green and light-blue ribbons, respectively. The two ligand molecules are shown in space-filling representation, with the carbon atoms of one molecule in green and the other in cyan. (B) Detailed view of one of the two **17c** binding sites. Colors are as in (A), with hydrogen bonds indicated as dashed orange lines. (C) The complex of TLR8 bound to **17c** is shown aligned to agonist-bound TLR8 (RCSB PDB 3W3J), orange color), apo TLR8 (3W3G, pink), and TLR8 bound to antagonist CU-CPT9b (SWYZ, purple).

which were subjected to cross-coupling with phenylboronic acids **14** to afford, after Boc deprotection, analogues **5a–p** and **7d,f**. Alternatively, **11a,c–f** were reacted with 3,4-dimethoxyphenylboronic acid under cross-coupling conditions, followed by Boc removal via treatment with HCl to give **6a** or **17c–f**.

Synthesis of C-3-trifluoroethylindole **17g** began with the reaction of 3,4-dimethoxybenzene with trifluoromethylbutanoic acid and polyphosphoric acid (PPA). The resulting intermediate was heated with 4-bromophenylhydrazine and PPA to afford **16**. A three-step sequence (coupling/hydrogenation/deprotection) analogous to that described for the conversion of **9** to **10** above was applied to **16** to afford **17g**. Reaction of intermediates **17** with acetyl chloride (**18**), alkyl

chlorides **19**, or aldehyde or ketones **20** afforded **6b–j**. Intermediates **6a/17c–g** were separately subjected to reductive with a subsequent Boc deprotection to give final compounds **7b,c,e–g**. *N*-Methylindole **7a** was prepared by reductive amination of **6a** and **12**, followed by exposure to sodium hydride and MeI prior to Boc removal.

In conclusion, we discovered **7f** as a promising lead for a small molecule TLR7/9 dual antagonist program aimed at the treatment of lupus and other autoimmune diseases. Through an HTS campaign, we identified a 2-phenyl-indole-5-piperidine series and conducted optimization studies, which led to the incorporation of dimethoxyphenyl substitution at C-2 to drive dual potency against TLR7 and TLR9. Potency was further

Scheme 1. Synthesis of TLR Antagonists^a

^aReagents and conditions: (a) LiAlH₄, THF, reflux, 45%; (b) Shvo's catalyst, amine, K₂CO₃, 155 °C, 21%–72%; (c) *tert*-butyl 4-(4,4,5,5-tetramethyl-1,3,2-dioxaborolan-2-yl)-3,6-dihydropyridine-1(2*H*)-carboxylate, 3.0 M K₃PO₄, Pd(dppf)Cl₂, THF, 70–84%; (d) 10% Pd/C, H₂, EtOAc, 85–97%; (e) NCS, DCM, 84%; (f) NBS, DCM then 10% aqueous Na₂SO₃, 20–75%; (g) HBr(AcOH), DCM; (h) TEA, AcOH, Na(OAc)₃BH, DCM, 85% 2-steps; (i) 3.0 M K₃PO₄, Pd(dppf)Cl₂, THF, then TFA, DCM, 2–66%; (j) 3.0 M K₃PO₄, 3,4-dimethoxyphenylboronic acid, Pd(dppf)Cl₂, THF, 1 h; (k) 4.0 M HCl in dioxane, 44–100% (2 steps); (l) trifluoromethylbutanoic acid, PPA, toluene, 43%; (m) 4-bromophenylhydrazine, PPA, 155 °C, 38%; (n) TEA, AcOH, Na(OAc)₃BH, DCM; (o) 4.0 M HCl in dioxane, 12–95%; (p) NaH, DMF, then MeI, then 50% TFA in DCM, 52%; (q) TEA, DCM, 25–73%; (r) DBU, DCM, 6%; (s) TEA, AcOH, Na(OAc)₃BH, DCM, 11–88%.

enhanced through modifications of alkyl substituents at C-3, while changes to C-5 provide an area for tuning of potency as well as PK and off-target liabilities through modification of compound basicity and polarity. The excellent potency and oral PK properties of 7f in mouse enabled its use in multiple in vivo models for the evaluation of modulating TLR7/9 driven pharmacodynamic responses (with TLR8 not able to be evaluated in mouse systems) and also for efficacy in rodent disease models for psoriasis and lupus. These results establish small molecule inhibition of the TLR7/9 pathway as a promising approach for treatment of autoimmune disorders.

■ ASSOCIATED CONTENT

Supporting Information

The Supporting Information is available free of charge at <https://pubs.acs.org/doi/10.1021/acsmchemlett.0c00264>.

Preparation and characterization of compounds 5–7; biologic assays. X-ray cocrystallographic data, and refinement statistics for compound 17c bound to TLR8 (PDF)

Accession Codes

Atomic coordinates for the X-ray structure of compound 17c: (PDB 6V9U) in TLR8 is available from the RCSB Protein Data Bank (www.rcsb.org). Authors will release the atomic coordinates upon article publication.

■ AUTHOR INFORMATION

Corresponding Author

Alaric J. Dyckman – Bristol Myers Squibb Research and Development, Princeton, New Jersey 08543, United States; orcid.org/0000-0002-1050-2077; Phone: 609-252-3593; Email: alaric.dyckman@bms.com

Authors

Christopher P. Mussari – Bristol Myers Squibb Research and Development, Princeton, New Jersey 08543, United States
 Dharmal S. Dodd – Bristol Myers Squibb Research and Development, Princeton, New Jersey 08543, United States
 Ratna Kumar Sreekantha – The Biocon Bristol Myers Squibb Research Center (BBRC), Bangalore 560099, India
 Laxman Pasunoori – The Biocon Bristol Myers Squibb Research Center (BBRC), Bangalore 560099, India
 Honghe Wan – Bristol Myers Squibb Research and Development, Princeton, New Jersey 08543, United States
 Shana L. Posy – Bristol Myers Squibb Research and Development, Princeton, New Jersey 08543, United States
 David Critton – Bristol Myers Squibb Research and Development, Princeton, New Jersey 08543, United States
 Stefan Ruepp – Bristol Myers Squibb Research and Development, Princeton, New Jersey 08543, United States
 Murali Subramanian – The Biocon Bristol Myers Squibb Research Center (BBRC), Bangalore 560099, India
 Andrew Watson – Bristol Myers Squibb Research and Development, Princeton, New Jersey 08543, United States

Paul Davies – Bristol Myers Squibb Research and Development, Princeton, New Jersey 08543, United States

Gary L. Schieven – Bristol Myers Squibb Research and Development, Princeton, New Jersey 08543, United States

Luisa M. Salter-Cid – Bristol Myers Squibb Research and Development, Princeton, New Jersey 08543, United States

Ratika Srivastava – The Biocon Bristol Myers Squibb Research Center (BBRC), Bangalore 560099, India; orcid.org/0000-0001-6308-553X

Debarati Mazumder Tagore – The Biocon Bristol Myers Squibb Research Center (BBRC), Bangalore 560099, India

Shailesh Dudhgaonkar – The Biocon Bristol Myers Squibb Research Center (BBRC), Bangalore 560099, India

Michael A. Poss – Bristol Myers Squibb Research and Development, Princeton, New Jersey 08543, United States

Percy H. Carter – Bristol Myers Squibb Research and Development, Princeton, New Jersey 08543, United States

Complete contact information is available at:

<https://pubs.acs.org/10.1021/acsmchemlett.0c00264>

Notes

The authors declare no competing financial interest.

ABBREVIATIONS

TLR, toll-like receptor; PRR, pattern recognition receptor; PAMP, pathogen-associated molecular patterns; DAMP, danger-associated molecular patterns; ECD, extracellular domain or ectodomain

REFERENCES

(1) Baccala, R.; Gonzalez-Quintal, R.; Lawson, B.; Stern, M.; Kono, D.; Beutler, B.; Theofilopoulos, A. Sensors of the innate immune system: Their mode of action. *Nat. Rev. Rheumatol.* **2009**, *5*, 448–456.

(2) O'Neill, L.; Golenbock, D.; Bowie, A. The history of Toll-like receptors — redefining innate immunity. *Nat. Rev. Immunol.* **2013**, *13*, 453–460.

(3) Marshak-Rothstein, A.; Rifkin, I. Immunologically active autoantigens: The role of Toll-like receptors in the development of chronic inflammatory disease. *Annu. Rev. Immunol.* **2007**, *25*, 419–441.

(4) Heil, F.; Hemmi, H.; Hochrein, H. Species specific recognition of single-stranded RNA via Toll-like receptor 7 and 8. *Science* **2004**, *303*, 1526–1529.

(5) Subramanian, S.; Tus, K.; Li, Q. Z.; Wang, A.; Tian, X. H.; Zhou, J.; Liang, C.; Bartov, G.; McDaniel, L. D.; Zhou, X. J.; Schultz, R. A.; Wakeland, E. K. A TLR7 translocation accelerates systemic autoimmunity in murine lupus. *Proc. Natl. Acad. Sci. U. S. A.* **2006**, *103*, 9970–9975.

(6) Christensen, S.; Shupe, J.; Nickerson, K.; Kashgarian, M.; Flavell, R.; Shlomchik, M. Toll-like receptor 7 and TLR9 dictate autoantibody specificity and have opposing inflammatory and regulatory roles in a murine model of lupus. *Immunity* **2006**, *25*, 417–428.

(7) Liu, J.; Xu, C.; Hsu, L.; Luo, Y.; Xiang, R.; Chuang, T. A five-amino-acid motif in the undefined region of the TLR8 ectodomain is required for species-specific ligand recognition. *Mol. Immunol.* **2010**, *47*, 1083–1090.

(8) Cervantes, J.; Weinerman, B.; Basole, C.; Salazar, J. TLR8: The forgotten relative revindicated. *Cell. Mol. Immunol.* **2012**, *9*, 434–438.

(9) Patinote, C.; Karroum, N.; Moarbess, G.; Cirnat, N.; Kassab, I.; Bonnet, P.; Deleuze-Masquéfa, C. Agonist And Antagonist Ligands Of Toll-Like Receptors 7 And 8: Ingenious Tools For Therapeutic Purposes. *Eur. J. Med. Chem.* **2020**, *193*, 112238.

(10) Kuźnik, A.; Benčina, M.; Švajger, U.; Jeras, M.; Rozman, B.; Jerala, R. Mechanism Of Endosomal TLR Inhibition By Antimalarial Drugs And Imidazoquinolines. *J. Immunol.* **2011**, *186*, 4794–4804.

(11) An, J.; Woodward, J.; Sasaki, T.; Minie, M.; Elkon, K. Cutting Edge: Antimalarial Drugs Inhibit IFN- β Production Through Blockade Of Cyclic GMP-AMP Synthase–DNA Interaction. *J. Immunol.* **2015**, *194*, 4089–4093.

(12) HEK-Blue TLR Cells; InvivoGen, 2019; <https://www.invivo-gen.com/hek-blue-tlr-cells> (accessed 2019-03-14).

(13) van der Fits, L.; Mourits, S.; Voerman, J.; Kant, M.; Boon, L.; Laman, J.; Cornelissen, F.; Mus, A.; Florencia, E.; Prens, E.; Lubberts, E. Imiquimod-induced psoriasis-like skin inflammation in mice is mediated via the IL-23/IL-17 axis. *J. Immunol.* **2009**, *182*, 5836–5845.

(14) Perry, D.; Sang, A.; Yin, Y.; Zheng, Y.; Morel, L. Murine models of systemic lupus erythematosus. *J. Biomed. Biotechnol.* **2011**, *2011*, 1–19.

(15) Tanji, H.; Ohto, U.; Shibata, T.; Miyake, K.; Shimizu, T. Structural reorganization of the Toll-like receptor 8 dimer induced by agonistic ligands. *Science* **2013**, *339*, 1426–1429.

(16) Tanji, H.; Ohto, U.; Shibata, T.; Taoka, M.; Yamauchi, Y.; Isobe, T.; Miyake, K.; Shimizu, T. Toll-like receptor 8 senses degradation products of single-stranded RNA. *Nat. Struct. Mol. Biol.* **2015**, *22*, 109–115.

(17) Zhang, S.; Hu, Z.; Tanji, H.; Jiang, S.; Das, N.; Li, J.; Sakaniwa, K.; Jin, J.; Bian, Y.; Ohto, U.; Shimizu, T.; Yin, H. Small-molecule inhibition of TLR8 through stabilization of its resting state. *Nat. Chem. Biol.* **2018**, *14*, 58–64.